URSI-RCRS 2024, ARIES/GEHU, Bhimtal, India, 22 - 25October, 2024

A Flexible Broadband Microwave Absorber with Resistive Ink

S. P. Mishra *(1), and S. Maity(1)
(1) National Institute of Technology, Rourkela
Department of Electronics and Communication Engineering, Odisha-769008, India

Abstract

The design and analysis of a flexible, broadband microwave absorber based on resistive ink technology is presented in this work. The design features ink patterns printed on a dielectric sheet, segregated from the ground plane by an air spacer (foam). The proposed structure is independent of the polarization angles because of its four-fold symmetry. The absorber spans a frequency range from 11.69 GHz to 31.06 GHz, providing an absorption bandwidth of 19.37 GHz. This range encompasses the entire Ku and K bands and part of the Ka-band. The periodicity and thickness of the unit cell is $0.31\lambda_l$ and $0.08\ \lambda_l$ respectively, where λ_l indicates the wavelength determined at the lowermost operating frequency of the absorber. The proposed configuration can be employed for applications such as reduction of electromagnetic interference, stealth technology, etc.

1. Introduction

A frequency-selective surface (FSS) is a periodic structure engineered to selectively absorb, reflect, or transmit electromagnetic waves. These stsructures have potential applications in spatial filtering [1], stealth technology [2], reduction of radar cross section [3], radomes [4], and absorbers [5]. Microwave absorbers utilizing Frequency Selective Surfaces (FSS) [6] are crucial in stealth technology for absorbing electromagnetic (EM) waves impinging on any target. During World War II, the Salisbury screen absorber [7] was introduced, utilizing the quarter-wave transformer matching methodology. The disadvantage of this configuration was its narrow absorption bandwidth. Jaumann absorber [8] employed multiple resistive layers separated from the ground plane by a distance of a quarter wavelength to enhance the absorption bandwidth. However, this configuration has a larger thickness compared to the Salisbury screen. Absorbers incorporating a frequency-selective surface placed at the top of a dielectric sheet, with a metallic sheet on the lower side of the substrate, have gathered significant interest from researchers. This is due to their improved performance compared to the other designs.

Losses generally play a huge role in the absorption of electromagnetic waves. The dielectric loss from the substrate and the conductive (ohmic) loss from metal patterns alone are insufficient to develop an effective absorber. To achieve broadband absorbers, various methods are employed, including the use of resistive sheet [9], resistive ink [10], and lumped resistors integrated into conductive patterns [11]. These methods increase the ohmic losses in the absorber design, thereby enhancing the absorption bandwidth. However, most of the works [12-13] have developed absorbers utilizing rigid substrates which has very less practical applications.

This manuscript presents a broadband, flexible microwave absorber. The absorber features resistive ink patterns printed on a flexible FR4 substrate, with a ground plane separated by the substrate using flexible foam. The proposed configuration is cost-effective, lightweight, and polarization-insensitive. It achieves broadband absorption from 11.69 GHz to 31.06 GHz, exhibiting a fractional bandwidth of 90.61% with respect to the centre frequency. To illustrate the wideband absorption, a plot of normalized impedance is included. Additionally, an equivalent circuit diagram is provided to simplify the design in terms of circuit parameters.

2. Absorber Design

The proposed configuration is made of a resistive ink pattern imprinted on the upper surface of a substrate, as depicted in Figure 1. The substrate (FR4) and the bottom surface of the absorber are separated by a flexible Foam (Figure 2). The thickness of the substrate ($\varepsilon_r = 4.4$, $\tan\delta = 0.02$) is 0.2 mm, while the thickness of the foam ($\varepsilon_r = 1, \tan\delta = 0$) is 2 mm. A commercially available resistive paint Yshield HSF-54 [14] is utilized, having a thickness of 35 μm and a conductivity of 664 S/m. In order to analyze an infinite array, floquet port excitation and lattice pair boundary conditions are applied to the unit cell. The whole setup is implemented in High-frequency structure simulator (HFSS). The performance of the structure under plane wave excitation is analyzed for transverse magnetic (TM) and transverse electric (TE) wave of propagation. The absorptivity in terms of co and cross reflection and transmission coefficients is defined as [15] :

$$A(\omega) = 1 - \left(|R_{xx}(\omega)|^2 + |R_{yx}(\omega)|^2\right) - \left(|T_{xx}(\omega)|^2 + |T_{yx}(\omega)|^2\right) \quad (1)$$

Here, $R_{xx}(\omega)$ and $T_{yx}(\omega)$ denotes the co-polarized reflection and transmission coefficient, respectively, while $R_{xx}(\omega)$ and $T_{yx}(\omega)$ denotes the co-polarized reflection and transmission coefficient, respectively. As the absorber is backed by a metallic plate, the above equation is modified as:

$$A(\omega) = 1 - \left(|R_{xx}(\omega)|^2 + |R_{yx}(\omega)|^2\right) \quad (2)$$

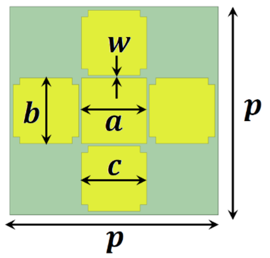

Figure 1. Top view of the unit cell with optimized parameters: $p = 7.97\ mm$, $a = 2.5\ mm$, $b = 2.5\ mm$, $c = 2\ mm$, $w = 2.6\ mm$, $h_1 = 0.2\ mm$, $h_2 = 2\ mm$

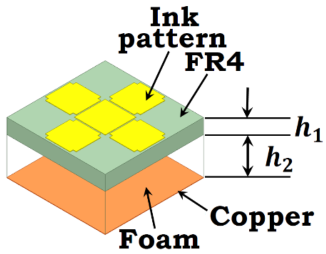

Figure 2. Isometric view of the unit cell

3. Results and Discussion

The magnitude of the cross- and co-polarized reflection coefficients for the unit cell is shown in Figure 3. For a normally incident EM wave, the configuration has a very low level of cross-polarized component due to the symmetrical design. The co-pol level is below -10 dB in the frequency span of 11.69 GHz to 31.06 GHz, showing that the impedance of the structure matches that of air.

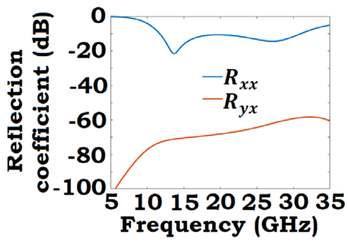

Figure 3. Co and cross-polarized reflection coefficients as a function of frequency

The absorptivity computed from (2) is illustrated in Figure 4. It is evident that in the frequency span of 11.69 GHz- 31.06 GHz, the proposed geometry can absorb the power (90%) of a normally incident EM wave. The absorber covers Ku (12 GHz- 18 GHz), K (18 GHz-27 GHz), and some parts of the Ka-band (27 GHz- 40 GHz).

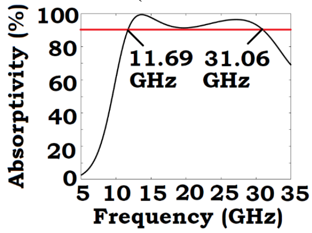

Figure 4. Response of the structure for a normally incident wave

To demonstrate the polarization-independent behaviour of the absorber, the absorptivity of the unit cell under normal incidence is computed by altering the polarization angle (φ), as illustrated in Figure 5. Based on Figure 5, it is clear that the response of the design is not affected by the polarization angle, demonstrating that the proposed absorber is polarization insensitive.

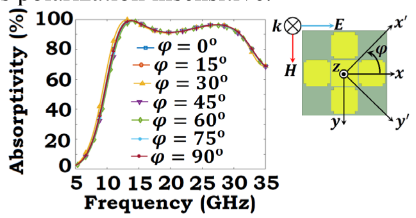

Figure 5. Absorptivity of the structure with change in polarization angle

The performance of the unit cell under oblique incidence for transverse electric and transverse magnetic waves are denoted in Figure 6 and Figure 7, respectively. The incident angle (θ) is varied from $0^o - 30^o$ for both cases. For transverse electric polarization, when the incident angle is increased to 15^o, the lower and the higher resonant frequency decreases. There is an increase and decrease in absorptivity level at the higher and the lower resonant frequency, respectively. For $\theta = 30^o$, the lower resonant frequency remains unchanged, while the higher resonant frequency increases. In both instances ($\theta = 15^o$ and $\theta = 30^o$), the 90% absorption bandwidth is less compared to the case of $\theta = 0^o$. However, the absorptivity curve remains greater than 80% in both cases. In the case of TM polarization, when θ is increased to 15^o the higher and the lower resonant frequency decrease with a reduction and enhancement in absorptivity level, respectively. The absorption bandwidth is lesser than in the case of $\theta = 0^o$. For $\theta = 30^o$, the absorptivity curve, when compared to normal incidence shifts right and also there is an enhancement in the absorption bandwidth.

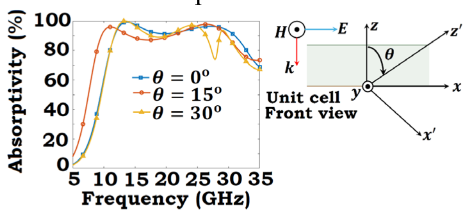

Figure 6. Absorptivity as a function of incident angle variation under TE mode

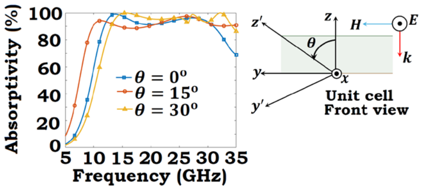

Figure 7. Absorptivity as a function of incident angle variation under TM mode

Figure 8 depicts the normalized impedance (Z_{in}) of the unit cell. From Figure 8, it is clearly seen that within the frequency range where the absorber is operating, the real part and imaginary part approach to unit and zero, respectively. This indicates that a perfect impedance matching is obtained between the absorber and the impedance of the air. The input impedance is computed using the following expression [16]:

$$Z_{in} = \sqrt{\frac{(1 + S_{11} + S_{21})^2 - (S_{31})^2}{(1 - S_{11} - S_{21})^2 - (S_{31})^2}} \quad (3)$$

Here, S_{11} and S_{21} denotes the scattering parameters corresponding to the reflected wave, while S_{31} is the scattering parameters corresponding to transmitted wave. As the bottom portion of the absorber is a metal sheet, the transmitted wave is neglected which leads to transformation of eq. (3) as follows:

$$Z_{in} = \frac{(1 + S_{11} + S_{21})}{(1 - S_{11} - S_{21})} \quad (4)$$

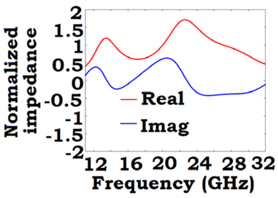

Figure 8. Variation of normalized impedance with frequency

To assess the impact of resistive ink on absorptivity, we replaced the ink pattern with a copper-based pattern, as illustrated in Figure 9. The results indicate that employing a copper-based pattern in the unit cell significantly reduces absorptivity and also the 90% absorption bandwidth. Conversely, both absorptivity and absorption bandwidth are enhanced when an ink pattern is utilized. The introduction of additional ohmic losses in the structure contributes to the improvement of the wide absorption bandwidth.

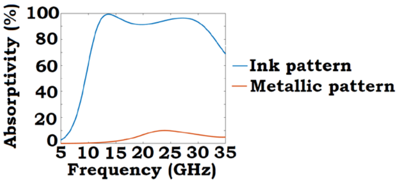

Figure 9. Effect of resistive ink and metal-based pattern on absorptivity

To evaluate the impact of the Foam sandwiched between the ground plane and the FR4 substrate, the spacer thickness (h_2) is adjusted from 2 to 5 mm. Increasing the height of the spacer shifts the absorption band toward the lower frequency range, accompanied by a decrease in the 90% absorption bandwidth. The optimized value of the thickness is 2 mm, as this configuration covers the required frequency bands, as shown in Figure 10.

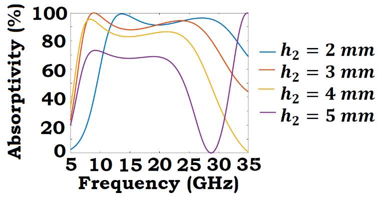

Figure10. Effect of the height of the air-spacer on the absorptivity

Table I compares the performance of the structure to that of similar studies published in the literature. The results reveal that the proposed configuration offers wider fractional bandwidth and a reduced structural thickness.

Table I

Comparative Analysis of Current Study with Previous Study

Ref.	Size of the unit cell	Thickness	Frequency range	Fractional bandwidth
[17]	$0.414\lambda_l$	$0.082\ \lambda_l$	8.00 GHz−13.00 GHz	51.16 %
[18]	$0.133\ \lambda_l$	$0.077\ \lambda_l$	8.00 GHz−18.00 GHz	76.92 %
[19]	$0.194\ \lambda_l$	$0.054\ \lambda_l$	10.45 GHz−17.64 GHz	51.19 %
[20]	$0.193\ \lambda_l$	$0.097\ \lambda_l$	5.8 GHz-12.2 GHz	71.1 %
[21]	$0.267\ \lambda_l$	$0.12\ \lambda_l$	8 GHz-18 GHz	76.9 %
[22]	$0.412\ \lambda_l$	$0.136\ \lambda_l$	24.7 GHz-38.8 GHz	44.4 %
This work	$0.31\lambda_l$	$0.08\ \lambda_l$	11.69 GHz-31.06 GHz	90.61 %

4. Conclusion

This article introduces a flexible, polarization-independent microwave absorber based on resistive ink methodology. The absorber consists of resistive patterns printed on a 0.2 mm thick FR4 sheet. The dielectric substrate is placed 2 mm above a metallic plate, with an air spacer in between. The proposed design achieves a 90% absorption bandwidth between 11.69 GHz and 31.06 GHz, resulting in a fractional bandwidth of 90.61%. The structure can cover the complete spectrum of the Ku and K bands, with some region of Ka-band. Since the absorber has a lower thickness, it can be wrapped on a curved surface.

7. References

1.F. Bayatpur and K. Sarabandi, “Multipole Spatial Filters Using Metamaterial-Based Miniaturized-Element Frequency-Selective Surfaces,” *IEEE Transactions on Microwave Theory and Techniques*, **56**, 12, 2008, pp. 2742-2747.

2. V. K. Chakradhary, H. B. Baskey, R. Roshan, A. Pathik and M. J. Akhtar, “Design of Frequency Selective Surface-Based Hybrid Nanocomposite Absorber for Stealth Applications,” *IEEE Transactions on Microwave Theory and Techniques*, **66**, 11, 2018, pp. 4737-4744.

3. S. R. Thummaluru, R. Kumar and R. K. Chaudhary, “Isolation Enhancement and Radar Cross Section Reduction of MIMO Antenna With Frequency Selective Surface,” *IEEE Transactions on Antennas and Propagation*, **66**, 3, 2018, pp. 1595-1600.

4. S. Narayan, G. Gulati, B. Sangeetha and R. U. Nair, “Novel Metamaterial-Element-Based FSS for Airborne Radome Applications,” *IEEE Transactions on Antennas and Propagation*, **66**, 9, 2018, pp. 4695-4707.

5. Z. Sun, L. Yan, X. Zhao and R. X. -K. Gao, “An Ultrawideband Frequency Selective Surface Absorber With High Polarization-Independent Angular Stability,” I*EEE Antennas and Wireless Propagation Letters*, **22**, 4, 2023, pp. 789-793.

6. B. A. Munk, *Frequency Selective Surfaces: Theory and Design*, NewYork, NY, USA: Wiley, 2000.

7. W. W. Salisbury, “Absorbent body for electromagnetic waves,” U.S. Patent 2599944, 1952.

8. L. J. Du Toit, “The design of Jauman absorbers,” *IEEE Antennas and Propagation Magazine*, **36**, 6, 1994,pp. 17-25.

9. J. Dong, Y. Ma and M. Wang, “An Ultrawideband Miniaturized Ultrathin Flexible Metamaterial Absorber Using Lightweight ITO Film,” *IEEE Antennas and Wireless Propagation Letters*, **22**, 12, 2023,pp. 2970-2974.

10. M. O. Placha, B. Salski, D. Janczak, P. R. Bajurko, W. Gwarek and M. Jakubowska, “A Broadband Absorber With a Resistive Pattern Made of Ink With Graphene Nano-Platelets,” *IEEE Transactions on Antennas and Propagation*, **63**, 2, 2015, pp. 565-572.

11. J. Chen, Y. Shang and C. Liao, “Double-Layer Circuit Analog Absorbers Based on Resistor-Loaded Square-Loop Arrays,” *IEEE Antennas and Wireless Propagation Letters*, **17**, 4, 2018, pp. 591-595.

12. V. P. Inbali, V. P. Sakthivel, C. Venkatesh, and T. R. Suresh Kumar, “Design of Broadband Circuit Analog Absorber With Optimal Thickness for Stable Angular Response in C, X, Ku, and K Bands,” *IEEE Transactions on Electromagnetic Compatibility*, **65**, 6, 2023, pp. 2065-2069.

13. D. Kundu, S. Baghel, A. Mohan and A. Chakrabarty, “Design and Analysis of Printed Lossy Capacitive Surface-Based Ultrawideband Low-Profile Absorber,” *IEEE Transactions on Antennas and Propagation*, **67**, 5, 2019, pp. 3533-3538.

14. Y-Shield EMR Protection. Accessed: Feb. 2018. [Online]. Available: http://www.yshield.com/

15. D. Kundu, A. Mohan, and A. Chakrabarty, “Comment on ‘wide - angle broadband microwave metamaterial absorber with octave bandwidth,” *IET Microwaves, Antennas & Propagation*, **11**, 3, 2016, pp. 442−443.

16. E. Celenk, C. Lynch, and M. M. Tentzeris, “An ultrawideband all-textile metamaterial absorber for Ku-, K-, and Ka-band applications,” *IEEE Antennas and Wireless Propagation Letters*, **23**, 6, 2024, pp. 1789–1793.

17. S. Ghosh, S. Bhattacharyya, D. Chaurasiya and K. V. Srivastava, “An Ultrawideband Ultrathin Metamaterial Absorber Based on Circular Split Rings,” *IEEE Antennas and Wireless Propagation Letters*, **14**, 2015, pp. 1172-1175.

18. D. Zhou, X. Huang and Z. Du, “Analysis and Design of Multilayered Broadband Radar Absorbing Metamaterial Using the 3-D Printing Technology-Based Method,” *IEEE Antennas and Wireless Propagation Letters*, **16**, 2017, pp. 133-136.

19. D. Sood and C. C. Tripathi, “A compact ultrathin ultra-wideband metamaterial microwave absorber,” *J. Microw. Optoelectron. Electromagn. Appl.*, **16**, 2, 2017, pp. 514–528.

20. T. Jang, H. Youn, Y. J. Shin, and L. J. Guo, “Transparent and flexible polarization-independent microwave broadband absorber,” *ACS Photon.*, **1**, 3, 2014, pp. 279–284.

21. Q. Zhou, X. Yin, F. Ye, R. Mo, Z. Tang, X. Fan, L. Cheng, L. Zhang, “Optically transparent and flexible broadband microwave metamaterial absorber with sandwich structure,” *Appl. Phys. A*, **125**, 2, 2019.

22. C. Zhang, J. Yang, W. Cao, W. Yuan, J. Ke, L. Yang, Q. Cheng, T. Cui, “Transparently curved metamaterial with broadband millimeter wave absorption,” *Photon. Res.*,**7**, 4, 2019, pp. 478–485.